

# Channel Estimation for mmWave Pinching-Antenna Systems

Gui Zhou<sup>§</sup>, Vasilis Papanikolaou<sup>§</sup>, Zhiguo Ding<sup>‡</sup>, and Robert Schober<sup>§</sup>

<sup>§</sup>Friedrich-Alexander-Universität Erlangen-Nürnberg, Germany

<sup>‡</sup> University of Manchester, UK

e-mail: {gui.zhou, vasilis.papanikolaou, robert.schober}@fau.de,

zhiguo.ding@manchester.ac.uk

## Abstract

The full potential of pinching-antenna systems (PAS) can be unblocked if pinching antennas can be accurately activated at positions tailored for the serving users', which means that acquiring accurate channel state information (CSI) at arbitrary positions along the waveguide is essential for the precise placement of antennas. In this work, we propose an innovative channel estimation scheme for millimeter-wave (mmWave) PAS. The proposed approach requires activating only a small number of pinching antennas, thereby limiting antenna switching and pilot overhead. Specifically, a base station (BS) equipped with a waveguide selectively activates subarrays located near and far from the feed point, each comprising a small number of pinching antennas. This configuration effectively emulates a large-aperture array, enabling high-accuracy estimation of multipath propagation parameters, including angles, delays, and path gains. Simulation results demonstrate that the proposed method achieves accurate CSI estimation and data rates while effectively reducing hardware switching and pilot overhead.

## Index Terms

Pinching antennas, channel estimation, millimeter wave, massive MIMO, AoA/AoD estimation.

## I. INTRODUCTION

Pinching-antenna technology has emerged as a promising solution for building large-scale reconfigurable arrays with minimal hardware cost. Inspired by DOCOMO's 2022 demonstration [1], where beam patterns were formed by placing simple dielectric pinching elements (e.g., plastic clips) along a waveguide, the pinching antenna system (PAS) concept [1], [2] enables flexible beam control by dynamically adjusting the array configurations, including the number and the

positions of the antennas. This low-cost, flexibly deployable design has sparked growing research interest in harnessing waveguide-based arrays for adaptive and efficient wireless communications.

The authors of [2] provided the first analytical framework to characterize the channel properties and path-loss mitigation capabilities of pinching antennas, further demonstrating their potential for supporting non-orthogonal multiple access (NOMA), multiple-input multiple-output (MIMO), and interference management in multi-waveguide scenarios. In [3], discrete placement of pinching antennas was considered, where a NOMA-assisted downlink PAS scenario was considered and a matching-theory-based algorithm was developed to optimize the number and positions of activated antennas for throughput maximization. Building on this foundation, [4] extended the investigation to multiuser MIMO settings, proposing joint hybrid beamforming and pinching-element placement strategies for both uplink and downlink, showing substantial throughput gains over conventional MIMO baselines.

Most existing studies on PAS primarily focused on communication performance analysis and optimization, and assumed the availability of perfect accurate channel state information (CSI). In PAS, a pinching antenna is expected to continuously vary its position within a designated area, implying that CSI at any arbitrary position, or across a dense set of predefined ports, must be known to fully exploit its potential. Consequently, conventional channel estimation methods designed for fixed-antenna systems become inapplicable due to the resulting high pilot and hardware overhead. Similarly, channel estimation techniques developed for fluid antenna systems (FAS) cannot be adopted, as they are tailored for a far-field channel model that depends only on angles of departure/arrival and path gains [5]. In contrast, PAS typically operate in the near-field due to the high frequency and the extended size of the waveguide, where users often lie within the Fresnel region; thus, a distance-dependent free-space channel model has to be adopted. To date, limited research has addressed CSI estimation for PAS. In [6], the user location was estimated and used for beam training, which is applicable to pure line-of-sight (LoS) only. In [7], a machine learning-based method was proposed to predict the CSI at all waveguide locations, but can incur substantial pilot overhead due to the  $10^5$  training samples required for training dataset construction. These challenges underscore the urgent need for low-cost, scalable channel estimation schemes tailored to the unique characteristics of PAS.

In this work, we address the channel estimation problem for a time-division duplexing (TDD) mmWave PAS, in which the base station (BS) is equipped with a waveguide to serve a user. Leveraging the sparse-scattering nature of mmWave channels, we propose a sparse array-assisted

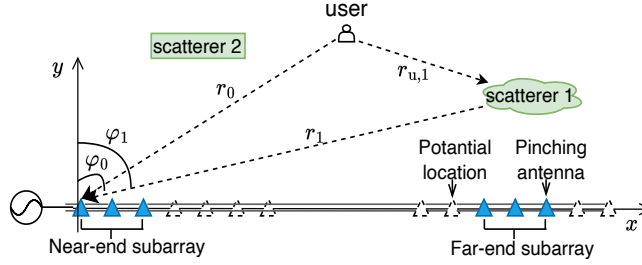


Fig. 1: System model for channel estimation.

multi-path channel reconstruction method, which involves four steps. First, by activating a few pinching antennas near the feed point, referred to as the near-end subarray, the BS receives pilot signals from the user to estimate the corresponding angles of arrival (AoAs). Second, by activating a few pinching antennas placed far from the feed point, forming the far-end subarray, the BS collects another set of pilot signals, from which the path distances are estimated based on the previously acquired AoAs. Third, the path gains are estimated by combining the signals received from both subarrays. Finally, utilizing the free-space steering vector model and the estimated sparse parameters, the full channel vector between all potential antenna positions on the waveguide and the user is reconstructed. Simulation results demonstrate that the proposed method provides highly accurate full CSI reconstruction, especially under strong LoS conditions (i.e., high Rician factor), while requiring low antenna switching and pilot overhead only.

**Notations:** The following mathematical notations and symbols are used throughout this paper. Vectors and matrices are denoted by boldface lowercase letters and boldface uppercase letters, respectively.  $\mathbf{X}^*$ ,  $\mathbf{X}^T$ , and  $\mathbf{X}^H$  denote the conjugate, transpose, and Hermitian (conjugate transpose) of matrix  $\mathbf{X}$ , respectively.  $\|\mathbf{x}\|_2$  denotes the L2-norm of vector  $\mathbf{x}$ .  $\text{Diag}(\mathbf{x})$  is a diagonal matrix with the entries of  $\mathbf{x}$  on its main diagonal. The Hadamard product between two matrices  $\mathbf{X}$  and  $\mathbf{Y}$  is denoted by  $\mathbf{X} \odot \mathbf{Y}$ .  $\mathbb{C}$  denotes the complex field,  $\mathbb{R}$  denotes the real field, and  $j \triangleq \sqrt{-1}$  is the imaginary unit. The notation  $\mathcal{CN}(a, b)$  refers to a circularly symmetric complex Gaussian distribution with mean  $a$  and variance  $b$ .

## II. SYSTEM MODEL

In this work, we consider a PAS assisted mmWave communication system where the BS is equipped with a dielectric waveguide of length  $L$ . Radiation elements are created by locally deforming the waveguide, i.e., applying pinching elements at one or multiple points, to induce controlled electromagnetic leakage for signal radiation, and are therefore termed pinching antennas. Let the radiation coefficient of the  $m$ th pinching antenna be denoted by  $w_m = e^{-j\beta x_m}$ ,

where  $x_m$  represents the distance from the feed point. Here,  $\beta = \eta_g \frac{2\pi}{\lambda}$  denotes the propagation constant of the waveguide, where  $\eta_g$  is the waveguide refractive index and  $\lambda$  is the free-space wavelength.

The configuration principle of the pinching array is to determine the optimal number and the optimal spatial locations of the pinching antennas on the waveguide, according to the predefined quality-of-service (QoS) metric, such as spectral efficiency, energy efficiency, or total power consumption. To enable optimal pinching array configuration, it is crucial that the CSI between any candidate position on the waveguide and the user is available at the BS, which motivates the design of channel estimation methods for PAS.

### A. Channel Model

Let  $M$  denote the number of candidate positions of the pinching elements on the waveguide. In theory,  $M$  could be arbitrarily large, since pinching elements may be positioned anywhere along the waveguide. However, for practical deployment and to ensure feasibility, the elements must be discretized at half-wavelength intervals, limiting  $M$  to  $M = \lfloor \frac{2L}{\lambda} \rfloor$ .

Assuming a short-range, high-frequency application, the wireless channel is modeled by a free-space sparse multiple path model, which includes a LoS path and  $P$  scattered paths<sup>1</sup>. Denote  $h_m$  by the channel coefficient between the  $m$ th candidate position and the user [8], where

$$h_m = \frac{\lambda}{4\pi r_{0,m}} e^{-j\frac{2\pi}{\lambda} r_{0,m}} + \frac{\lambda}{(4\pi)^{3/2}} \sum_{p=1}^P \frac{\alpha_p}{r_{p,m} r_{u,p}} e^{-j\frac{2\pi}{\lambda} (r_{p,m} + r_{u,p})}, \quad (1)$$

with  $\alpha_p > 0$  being the radar cross section (RCS) of scatterer  $p$ .  $r_{0,m}$  and  $r_{p,m}$  represent the physical distances from the user and the  $p$ th scatterer, respectively, to the  $m$ th candidate position on the waveguide.  $r_{u,p}$  is the physical distance from the user to the  $p$ th scatterer. Without loss of generality, assume that the waveguide is placed along the  $x$ -axis of the  $xy$ -plane, with its feed point located at the origin. For this setup, the distance from the  $p$ th scatterer or the user to the  $m$ -th candidate position is given by  $r_{p,m} = \sqrt{r_p^2 - 2r_p x_m \sin \varphi_p + x_m^2}$  for  $0 \leq p \leq P$ , where  $\varphi_p$  denotes the AoA at a reference point and  $r_p$  represents the distance to the reference point. Correspondingly, the distance  $r_{u,p}$  is calculated as  $r_{u,p} = \sqrt{r_0^2 - 2r_0 r_p \cos(\varphi_0 - \varphi_p) + r_p^2}$ , for  $1 \leq p \leq P$ . Without loss of generality, we designate the first candidate location, which also corresponds to the feed point, as the reference point, as shown in Fig. 1. Thus, we have  $r_p = r_{p,1}$ , for  $0 \leq p \leq P$ .

<sup>1</sup>For simplicity, it is assumed that the same scatterers are visible for the whole waveguide.

## B. LS Channel Estimation

To acquire the full CSI, denoted by  $\mathbf{h} = [h_1, \dots, h_M]^T$ , a straightforward approach is to apply the least squares (LS) method given the received signals at all candidate locations. Specifically, the user transmits pilot signal  $s(t)$  over  $M$  time slots, during which the BS sequentially activates a pinching antenna at each of the  $M$  candidate positions for signal reception. By collecting the received signals over the  $M$  time slots, the signal observed at the BS can be expressed as

$$\begin{aligned} \mathbf{y} &= [y(1), y(2), \dots, y(M)]^T = \mathbf{w} \odot \mathbf{h} \odot \mathbf{s} + \mathbf{z} \\ &= \text{diag}(\mathbf{w} \odot \mathbf{s})\mathbf{h} + \mathbf{z}, \end{aligned} \quad (2)$$

where  $\mathbf{w} = [w_1, \dots, w_M]^T$ ,  $\mathbf{s} = [s(1), \dots, s(M)]^T$ , constrained by transmit power  $q = \|\mathbf{s}\|_2^2$ , and  $\mathbf{z}$  denotes the additive white Gaussian noise (AWGN) vector with independent identically distributed (i.i.d.) entries following  $\mathcal{CN}(0, \sigma^2)$  with noise power  $\sigma^2$ . Assuming that all pilot signals are non-zero, the LS estimate of  $\mathbf{h}$  is given by

$$\hat{\mathbf{h}}_{\text{LS}} = \text{diag}(\mathbf{w} \odot \mathbf{s})^{-1}\mathbf{y}. \quad (3)$$

For simple point-to-point signal models such as (2), the LS estimator in (3) achieves high estimation accuracy, approaching the Cramér–Rao Bound (CRB) in the high signal-to-noise ratio (SNR) regime. However, this comes at the cost of substantial pilot overhead, which scales linearly with the number of candidate locations  $M$ .

## C. Geometric Channel Structure

To address this issue, we exploit the geometric structure of the channel vector  $\mathbf{h}$  based on (1), which can be rewritten as

$$\mathbf{h} = \sum_{p=0}^P \beta_p \mathbf{a}(r_p, \varphi_p),$$

where the complex path gains are given by  $\beta_0 = \frac{\lambda}{4\pi r_0} e^{-j\frac{2\pi}{\lambda} r_0}$  and  $\beta_p = \frac{\lambda \alpha_p}{(4\pi)^{3/2} r_p r_{u,p}} e^{-j\frac{2\pi}{\lambda} (r_p + r_{u,p})}$ ,  $1 \leq p \leq P$ . Here,  $\mathbf{a}(r_p, \varphi_p) \in \mathbb{C}^M$  denotes the general near-field array response vector [9], given by

$$\mathbf{a}(r_p, \varphi_p) = \left[ 1, \frac{r_p}{r_{p,2}} e^{-j\frac{2\pi}{\lambda} (r_{p,2} - r_p)}, \dots, \frac{r_p}{r_{p,M}} e^{-j\frac{2\pi}{\lambda} (r_{p,M} - r_p)} \right]^T, \quad (4)$$

which depends on the user location for  $p = 0$  and the scatterer positions for  $1 \leq p \leq P$ . The CSI for each path can be fully characterized by estimating the parameter triplet  $\{\beta_p, r_p, \varphi_p\}$ . In other words, estimating  $3P$  parameters suffices, eliminating the need to estimate all  $M$  individual channel entries. This leads to a classical sparse parametric estimation problem.

Motivated by near-field sparse channel estimation, the angles and distances of each path can be estimated based on the near-field steering vector (4) using existing techniques such as codebook-based search [10] or subspace methods like MUSIC [11]. To use (4), however, requires at least  $N$  pinching antennas uniformly distributed along the waveguide with half-wavelength spacing, such that the aperture  $D$  of the activated pinching array satisfies the Fresnel condition  $d = \frac{2D^2}{\lambda} \geq \max\{r_p\}_{p=1}^P$ . For example, at 28 GHz and a maximum target distance of 50 m, the required critical number of pinching antennas is  $N = 1 + \sqrt{\frac{8r}{\lambda}} \approx 195$ . This number is still substantial and, in practice, an even larger  $N$  is needed to ensure estimation accuracy. Therefore, it becomes essential to develop channel estimation algorithms that not only reduce the required pilot overhead and the required number of activated pinching antennas, but also ensure reliable estimation accuracy.

### III. PROPOSED ESTIMATION METHOD

In this section, inspired by sparse array design, we propose a scheme that activates a small number of sparsely distributed pinching antennas from the candidate locations to construct a large effective aperture. The selected antennas are divided into two subarrays: a near-end subarray with  $M_1$  elements placed close to the feed point for angle estimation, and a far-end subarray with  $M_2$  elements positioned farther away for distance estimation assisted by the estimated angles, as illustrated in Fig. 1. The path gains are then recovered by jointly processing the signals from both subarrays.

For the near-end subarray, the first  $M_1$  candidate locations are selected and the corresponding pinching antennas are activated one by one. The BS sequentially receives  $M_1$  pilot signals from these antennas, such that the received signal is given by

$$\mathbf{y}_{\text{ne}} = \text{diag}(\mathbf{w}_{\text{ne}} \odot \mathbf{s}_{\text{ne}})\mathbf{h}_{\text{ne}} + \mathbf{z}_{\text{ne}}, \quad (5)$$

where  $\mathbf{h}_{\text{ne}}$  and  $\mathbf{w}_{\text{ne}}$  are the channel and radiation vectors associated with the near-end subarray, corresponding to the first  $M_1$  entries of  $\mathbf{h}$  and  $\mathbf{w}$ , respectively.  $\mathbf{s}_{\text{ne}} = [s(1), \dots, s(M_1)]^T$  contains the pilot signals, and  $\mathbf{z}_{\text{ne}}$  is the AWGN vector at the near-end subarray.

Subsequently, the BS activates pinching antennas at candidate locations indexed from  $m_{\text{fe}}$  to  $m_{\text{fe}} + M_2 - 1$ , where  $m_{\text{fe}}$  is positioned near the far end of the waveguide, receiving the pilot signal  $\mathbf{s}_{\text{fe}} = [s(M_1 + 1), \dots, s(M_1 + M_2)]^T$ . The received signal is given by

$$\mathbf{y}_{\text{fe}} = \text{diag}(\mathbf{w}_{\text{fe}} \odot \mathbf{s}_{\text{fe}}) \mathbf{h}_{\text{fe}} + \mathbf{z}_{\text{fe}}, \quad (6)$$

where  $\mathbf{h}_{\text{fe}}$  and  $\mathbf{w}_{\text{fe}}$  denote the channel and radiation vectors associated with the far-end subarray, corresponding to entries  $m_{\text{fe}}$  through  $m_{\text{fe}} + M_2 - 1$  of  $\mathbf{h}$  and  $\mathbf{w}$ , respectively.  $\mathbf{z}_{\text{fe}}$  represents the corresponding AWGN vector. The total power of the pilot signal is constrained by  $q = \|\mathbf{s}_{\text{ne}}\|_2^2 + \|\mathbf{s}_{\text{fe}}\|_2^2$ .

#### A. Coarse Estimation of Angles and Distances

We begin by providing a higher-order approximation of the path distance [9]:

$$r_{p,m} \approx r_p - x_m \sin \varphi + \frac{x_m^2 \cos^2 \varphi}{2r_p} + \mathcal{O}(x_m^3). \quad (7)$$

*Angle Estimation:* The near-end subarray is used to accomplish angle estimation by an approximation based on the far-field steering channel model, as explained in the following. Since  $x_m$  is small compared to distance  $r_p$ , the higher-order terms  $\mathcal{O}(x_m^2) = \frac{x_m^2 \cos^2 \varphi}{2r_p}$  and  $\mathcal{O}(x_m^3)$  are negligible. Thus, the distance can be modelled by the first-order Taylor approximation, as  $r_{p,m} \approx r_{p,m}^{\text{first}} = r_p - x_m \sin \varphi_p$ ,  $1 \leq m \leq M_1$ . Additionally, the free-space path loss ratio  $\frac{r_p}{r_{p,M_1}} \approx 1$  is identical for the first  $M_1$  antennas, due to their spatial proximity. Under these approximations, the steering vector for the near-end subarray can be approximated by a distance-independent far-field steering vector, given by

$$\mathbf{a}_{\text{first}}^{\text{ne}}(\varphi_p) = \left[ 1, e^{-j\frac{2\pi}{\lambda}(-x_2 \sin \varphi_p)}, \dots, e^{-j\frac{2\pi}{\lambda}(-x_{M_1} \sin \varphi_p)} \right]^T. \quad (8)$$

Consequently, estimating the  $P + 1$  AoAs from (5) can be formulated as a  $(P + 1)$ -sparse reconstruction problem, which cannot be solved using the LS due to the nonlinear relationship between the vector in (8) and the AoAs. Here, we estimate the AoAs by using the low-complexity orthogonal matching pursuit (OMP) algorithm, where the dictionary matrix is constructed from the manifold vectors derived in (8):

$$\begin{aligned} \mathbf{C}_{\text{first}}^{\text{ne}} &\in C^{M_1 \times C_{\text{ne}}} \\ &= \left[ \mathbf{a}_{\text{first}}^{\text{ne}}\left(-\frac{\pi}{2}\right), \mathbf{a}_{\text{first}}^{\text{ne}}\left(-\frac{\pi}{2} + \frac{\pi}{C_{\text{ne}}}\right), \dots, \mathbf{a}_{\text{first}}^{\text{ne}}\left(\frac{\pi}{2} - \frac{\pi}{C_{\text{ne}}}\right) \right], \end{aligned} \quad (9)$$

where  $C_{\text{ne}}$  is the size of the dictionary and  $-\frac{\pi}{2} + \frac{\pi c}{C_{\text{ne}}}$  is the angle for the  $(c + 1)$ th steering vector. The estimated AoAs are denoted by  $\{\hat{\varphi}_p\}_{p=1}^P$ .

*Distance Estimation:* For the far-end subarray, the index  $m_{\text{fe}}$  is large and usually on the order of several hundreds, making the second- and third-order terms in (7) significant and thus non-negligible<sup>2</sup>. Therefore, higher-order effects must be considered, and the far-end subarray must retain the full free-space near-field steering vector as in (4), given by

$$\mathbf{a}^{\text{fe}}(\varphi_p, r_p) = \left[ \frac{r_p}{r_{p, m_{\text{fe}}}} e^{-j \frac{2\pi}{\lambda} (r_{p, m_{\text{fe}}} - r_p)}, \frac{r_p}{r_{p, m_{\text{fe}}+1}} e^{-j \frac{2\pi}{\lambda} (r_{p, m_{\text{fe}}+1} - r_p)}, \dots, \frac{r_p}{r_{p, m_{\text{fe}}+M_2-1}} e^{-j \frac{2\pi}{\lambda} (r_{p, m_{\text{fe}}+M_2-1} - r_p)} \right]^{\text{T}}, \quad (10)$$

where  $r_{p,m} = \sqrt{r_p^2 - 2r_p x_m \sin \varphi_p + x_m^2}$ , for  $m_{\text{fe}} \leq m \leq m_{\text{fe}} + M_2 - 1$ .

Given the estimated AoAs  $\{\hat{\varphi}_p\}_{p=1}^P$ , the steering vector in (10) becomes a function of the distance  $r_p$  only. Accordingly, we estimate  $r_p$  using the OMP algorithm with a distance-dependent dictionary defined as

$$\mathbf{C}^{\text{fe}}(\hat{\varphi}_p) = [\mathbf{a}^{\text{fe}}(\hat{\varphi}_p, d_{\text{min}}), \mathbf{a}^{\text{fe}}(\hat{\varphi}_p, d_{\text{min}} + \Delta d), \dots, \mathbf{a}^{\text{fe}}(\hat{\varphi}_p, d_{\text{max}} - \Delta d)] \in C^{M_2 \times C_{\text{fe}}}, \quad (11)$$

where  $C_{\text{fe}}$  is the dictionary size and  $\Delta d = \frac{d_{\text{max}} - d_{\text{min}}}{C_{\text{fe}} - 1}$  denotes the distance resolution from the range  $[d_{\text{min}}, d_{\text{max}}]$ . Each column  $\mathbf{a}^{\text{fe}}(\hat{\varphi}_p, d_{\text{min}} + c\Delta d)$  is generated from (10) using the angle  $\hat{\varphi}_p$  and a discrete distance value. The estimated distances are denoted by  $\{\hat{r}_p\}_{p=1}^P$ .

## B. Refined Estimation of Angles and Distances

The first-order Taylor approximation in (8) may still introduce non-negligible phase errors. For instance, substituting  $m = 40$  in Footnote 1 yields a second-order term of  $\mathcal{O}(x_m^2) = \frac{x_m^2 \cos^2 \varphi_p}{2r_p} = 0.0023$ , which results in an estimated angle of  $\hat{\varphi}_p = -0.0108$  when using  $\mathbf{C}_{\text{first}}^{\text{ne}}$  in (9) such that  $x_m \sin \hat{\varphi}_p = x_m \sin \varphi_p - \frac{x_m^2 \cos^2 \varphi_p}{2r_p}$ . This indicates a maximum angle estimation error of  $\varphi - \hat{\varphi}_p = 0.0108$  at  $r_p = 10$  m. Since the distance estimates  $\{\hat{r}_p\}_{p=1}^P$  are already available, the accuracy of angle estimation can be further enhanced by utilizing the second-order Taylor approximation of the distance, i.e.,  $r_{p,m} \approx r_{p,m}^{\text{se}} = r_p - x_m \sin \varphi_p + \frac{x_m^2 \cos^2 \varphi_p}{2r_p}$ , for  $1 \leq m \leq M_1$ , which reduces the phase approximation error in vector (8) for the near-end subarray.

<sup>2</sup>For instance, when  $r_p = 10$  m,  $\varphi_p = 0$ ,  $f_c = 28$  GHz and  $m_{\text{fe}} = 400$ , the second-order term is  $\mathcal{O}(x_{m_{\text{fe}}}^2) = \frac{x_{m_{\text{fe}}}^2 \cos^2 \varphi_p}{2r_p} = 0.2333$ .



Specifically, we update the angle-related dictionary denoted by  $\mathbf{C}_{\text{se}}^{\text{ne}}$ , where each column is generated using the following steering vector

$$\mathbf{a}_{\text{se}}^{\text{ne}}(\theta, \hat{r}_p) = \left[ 1, e^{-j\frac{2\pi}{\lambda}(-x_2 \sin \theta + \frac{x_2^2 \cos^2 \theta}{2\hat{r}_p})}, \dots, e^{-j\frac{2\pi}{\lambda}(-x_{M_1} \sin \theta + \frac{x_{M_1}^2 \cos^2 \theta}{2\hat{r}_p})} \right]^T. \quad (12)$$

After obtaining the refined angle estimates, denoted by  $\{\hat{\varphi}_p^{\text{se}}\}_{p=1}^P$ , using  $\mathbf{C}_{\text{se}}^{\text{ne}}$  in the OMP, the distances are re-estimated accordingly, yielding the refined distance estimates  $\{\hat{r}_p^{\text{se}}\}_{p=1}^P$ .

### C. Path Gain Estimation

By stacking the signals received by the near- and far-end subarrays, the overall observation can be expressed as

$$\begin{aligned} \mathbf{y}_{\text{n-f}} &= \begin{bmatrix} \mathbf{y}_{\text{ne}} \\ \mathbf{y}_{\text{fe}} \end{bmatrix} \\ &\triangleq \text{diag} \left( \underbrace{\begin{bmatrix} \mathbf{w}_{\text{ne}} \\ \mathbf{w}_{\text{fe}} \end{bmatrix}}_{\mathbf{w}_{\text{n-f}}} \odot \underbrace{\begin{bmatrix} \mathbf{s}_{\text{ne}} \\ \mathbf{s}_{\text{fe}} \end{bmatrix}}_{\mathbf{s}_{\text{n-f}}} \right) \underbrace{\begin{bmatrix} \mathbf{h}_{\text{ne}} \\ \mathbf{h}_{\text{fe}} \end{bmatrix}}_{\mathbf{h}_{\text{n-f}}} + \underbrace{\begin{bmatrix} \mathbf{z}_{\text{ne}} \\ \mathbf{z}_{\text{fe}} \end{bmatrix}}_{\mathbf{z}_{\text{n-f}}} \\ &\triangleq \text{diag}(\mathbf{w}_{\text{n-f}} \odot \mathbf{s}_{\text{n-f}}) \mathbf{A}_{\text{n-f}} \mathbf{b} + \mathbf{z}_{\text{n-f}}, \end{aligned}$$

where  $\mathbf{b} = [\beta_1, \dots, \beta_P]^T$  denotes the path gain vector, and  $\mathbf{A}_{\text{n-f}} = [\mathbf{a}_1^{\text{n-f}}, \dots, \mathbf{a}_P^{\text{n-f}}]$  is the combined steering matrix, with each  $\mathbf{a}_p^{\text{n-f}}$  containing the corresponding entries from the full steering vector  $\mathbf{a}_p$ .

Substituting the refined angle and distance estimates  $\{\hat{\varphi}_p^{\text{se}}\}_{p=1}^P$  and  $\{\hat{r}_p^{\text{se}}\}_{p=1}^P$  into  $\mathbf{A}_{\text{n-f}}$  yields the estimated matrix  $\hat{\mathbf{A}}_{\text{n-f}}$ . The LS estimate of path gain vector  $\mathbf{b}$  is then given by

$$\hat{\mathbf{b}} = \left( \text{diag}(\mathbf{w}_{\text{n-f}} \odot \mathbf{s}_{\text{n-f}}) \hat{\mathbf{A}}_{\text{n-f}} \right)^{-1} \mathbf{y}_{\text{n-f}}. \quad (13)$$

#### D. Channel Reconstruction

Once the AoAs, distances, and channel gains are estimated, we can reconstruct  $\mathbf{h}$  based on the free-space geometric model. In particular, we have

$$\hat{\mathbf{h}} = \sum_{p=0}^P \hat{\beta}_p \mathbf{a}_p(\hat{r}_p^{\text{se}}, \hat{\varphi}_p^{\text{se}}), \quad (14)$$

where  $\mathbf{a}_p(\hat{r}_p, \hat{\varphi}_p)$  can be calculated based on (4). The overall channel estimation algorithm is summarized in Algorithm 1.

---

#### Algorithm 1 Proposed Estimation Based on Sparse Array

---

**Input:**  $\mathbf{y}_{\text{ne}}, \mathbf{y}_{\text{fe}}, \mathbf{C}_{\text{first}}^{\text{ne}}, \mathbf{C}_{\text{se},p}^{\text{ne}}$ , and  $\mathbf{C}_p^{\text{fe}}$ .

- 1: Estimate AoAs  $\{\hat{\varphi}_p\}_{p=1}^P$  using OMP with dictionary  $\mathbf{C}_{\text{first}}^{\text{ne}}$ .
- 2: Estimate distances  $\{\hat{r}_p\}_{p=1}^P$  by constructing dictionary  $\{\mathbf{C}^{\text{fe}}(\hat{\varphi}_p)\}_{p=1}^P$  and applying OMP.
- 3: Estimate AoAs  $\{\hat{\varphi}_p^{\text{se}}\}_{p=1}^P$  by constructing dictionary  $\{\mathbf{C}_{\text{se}}^{\text{ne}}(\hat{r}_p)\}_{p=1}^P$  and using OMP.
- 4: Estimate distances  $\{\hat{r}_p^{\text{se}}\}_{p=1}^P$  by constructing dictionary  $\{\mathbf{C}^{\text{fe}}(\hat{\varphi}_p^{\text{se}})\}_{p=1}^P$  and applying OMP.
- 5: Estimate path gains  $\hat{\mathbf{b}}$  using (13).

**Output:**  $\hat{\mathbf{h}} = \sum_{p=0}^P \hat{\beta}_p \mathbf{a}_p(\hat{r}_p^{\text{se}}, \hat{\varphi}_p^{\text{se}})$ .

---

## IV. SIMULATION RESULTS

In this section, we present extensive simulation results to evaluate the performance of the proposed full CSI reconstruction method. A waveguide of length 3 meters operating at a carrier frequency of 28 GHz is considered. The waveguide refractive index is  $\eta_g = 1.4$ . The user is located at a distance of 5 m, and the distances of the  $P = 2$  scatterers are randomly drawn from the range [3, 10] m. The angles of the multipath components are randomly drawn from the interval  $[-\pi/2, \pi/2]$ . The noise power is set to  $-100$  dBm, and the starting index of the far-end subarray is set to  $m_{\text{fe}} = 450$ . Unless otherwise specified, the subarray sizes are configured as  $M_1 = M_2 = 30$ .

We evaluate two metrics: 1) the normalized mean square error (NMSE) of the full CSI, defined as  $\text{NMSE} = \mathbb{E} \left\{ \frac{\|\hat{\mathbf{h}} - \mathbf{h}\|_2^2}{\|\mathbf{h}\|_2^2} \right\}$ , where the expectation is taken over different channel realizations. 2) the data rate, calculated as  $\text{Rate} = \log_2 \left( 1 + \frac{q_c |w_{m_{\text{opt}}} h_{m_{\text{opt}}}|^2}{\sigma^2} \right)$ , with  $q_c = 40$  dBm denoting the transmit power for communication, and  $m_{\text{opt}}$  being the optimal pinching antenna index based on the estimated full CSI  $\hat{\mathbf{h}}$ . We evaluate four algorithms: Pro. Refine, which reconstructs the full CSI using refined angle and distance estimates via (14); Pro. Coarse, which estimates the path gains and reconstructs the CSI using coarse estimates  $\{\hat{\varphi}_p\}_{p=1}^P$  and  $\{\hat{r}_p\}_{p=1}^P$ , serving as a

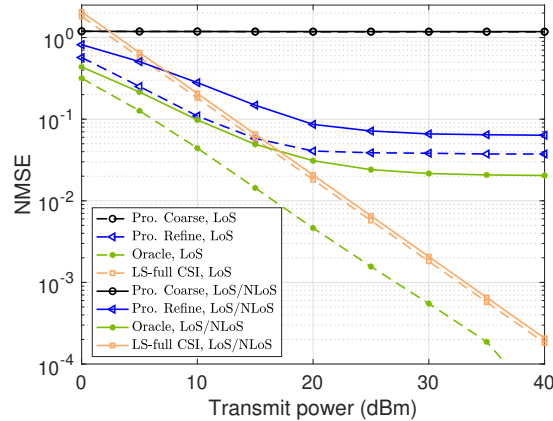


Fig. 2: NMSE versus transmit power.

performance lower bound; Oracle, which assumes perfect angle knowledge available at the BS while estimating the distances and path gains in Steps 2 and 5 of Algorithm 1, respectively, thereby representing an upper bound on performance; and LS-full CSI, which directly estimates the full CSI using the LS method in (3) with  $M = 2L/\lambda = 560$  pinching antennas, and serves as a benchmark. To ensure a fair comparison, the transmit power of the pilot signal is kept constant across all schemes. Accordingly, the pilot signal is set as  $s(t) = q/M$  for the LS method, and as  $s(t) = q/(M_1 + M_2)$  for the pilot signals used in the remaining schemes.

Fig. 2 illustrates the NMSE performance as a function of transmit power for different channel reconstruction methods. As can be observed, the proposed refined estimation approach significantly improves the accuracy compared to the coarse estimation approach. However, the refined method suffers a slight performance degradation compared to the Oracle scheme, indicating that the accuracy of angle estimation has a non-negligible impact on the subsequent distance and gain estimation. The proposed scheme outperforms the LS method for low transmit powers, while exhibiting a saturation effect at higher power levels due to the use of the OMP algorithm, whose reliance on a predefined dictionary makes it inherently vulnerable to grid mismatch, thus limiting estimation accuracy. As expected, the LS achieves high estimation accuracy at high transmit power, but at the cost of activating a large number of antennas and significant pilot overhead.

In Fig. 3, the data rate corresponding to the estimated full CSI is shown as a function of the transmit power in Fig. 2. In a mixed LoS/NLoS environment, the proposed refined estimation method outperforms the LS method when the transmit power is  $\leq 20$  dBm. Although the LS method eventually outperforms the proposed approach as transmit power increases, the refined

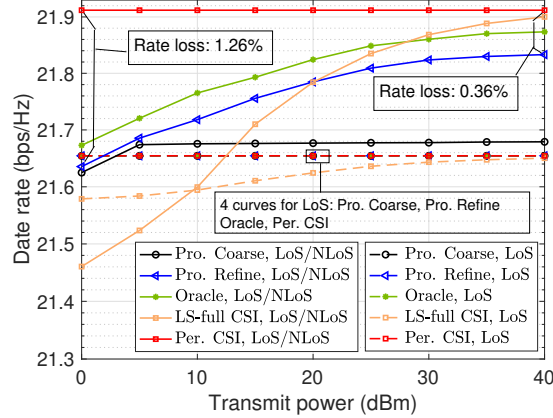


Fig. 3: Data rate versus transmit power.

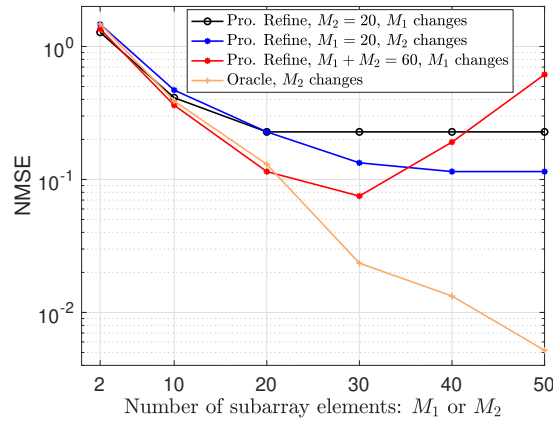


Fig. 4: NMSE versus the number of pinching antennas, when  $q = 40$  dBm.

method exhibits a minimal rate loss of only 0.36% compared to the perfect CSI case, achieving near-optimal performance. In the pure LoS scenario, the data rate from the three geometry-based estimation schemes exactly matches that under perfect CSI. This is likely because the selected index  $m_{\text{opt}}$  lies close to the truly optimal index  $m_{\text{per}}$  derived for perfect CSI. As a result, the received signals at these two locations differ only in phase, not in magnitude, resulting in the same date rate. In contrast, the LS method estimates each CSI entry independently, making  $m_{\text{opt}}$  more likely to deviate from the neighborhood of  $m_{\text{per}}$ , resulting in a larger performance gap at low transmit powers.

Fig. 4 shows the impact of the number of activated pinching antennas in the subarrays. For a fixed value on the  $x$ -axis, the total number of activated elements is identical for both the black and blue curves. As can be observed, configurations with  $M_1 > M_2$  consistently outperform those

with  $M_1 < M_2$ . This is because that allocating more antennas to the near-end subarray enhances angle estimation, thereby reducing the error propagated to the subsequent distance estimation. In contrast, prioritizing the far-end subarray for improved distance estimation is less effective. Furthermore, the red curve shows that, when the total number of subarray antennas is fixed, an equal allocation between the two subarrays achieves the best overall estimation accuracy.

## V. CONCLUSION

In this work, we proposed a novel channel estimation scheme for mmWave PAS. A sparse large-aperture array is constructed by activating a small number of pinching antennas at both the near and far ends of the waveguide relative to the feed point. The pilot signals received by the near-end subarray are utilized to estimate the angles of arrival, while those received by the far-end subarray are used to estimate propagation distances. The path gain estimation are then based on all the received pilot signals. Simulation results validate the effectiveness of the proposed scheme in acquiring accurate CSI with reduced hardware complexity.

## REFERENCES

- [1] A. Fukuda, H. Yamamoto, H. Okazaki, Y. Suzuki, and K. Kawai, "Pinching antenna: Using a dielectric waveguide as an antenna," *NTT DOCOMO Technical J.*, vol. 23, no. 3, pp. 5–12, Jan. 2022.
- [2] Z. Ding, R. Schober, and H. V. Poor, "Flexible-antenna systems: A pinching-antenna perspective," *IEEE Trans. Commun.*, pp. 1–1, Mar. 2025, Early Access.
- [3] K. Wang, Z. Ding, and R. Schober, "Antenna activation for NOMA assisted pinching-antenna systems," *IEEE Commun. Lett.*, Mar. 2025, Early Access.
- [4] A. Bereyhi *et al.*, "MIMO-PASS: Uplink and downlink transmission via MIMO pinching-antenna systems," Mar. 2025.
- [5] H. Xu *et al.*, "Channel estimation for FAS-assisted multiuser mmWave systems," *IEEE Commun. Lett.*, Mar. 2024.
- [6] S. Lv, Y. Liu, and Z. Ding, "Beam training for pinching-antenna systems (pass)," Feb. 2025.
- [7] J. Xiao, J. Wang, and Y. Liu, "Channel estimation for pinching-antenna systems (PASS)," Mar. 2025.
- [8] Z. Dong, X. Li, and Y. Zeng, "Characterizing and utilizing near-field spatial correlation for XL-MIMO communication," *IEEE Trans. Commun.*, vol. 72, no. 12, pp. 7922–7937, Dec. 2024.
- [9] H. Lu *et al.*, "A tutorial on near-field XL-MIMO communications toward 6G," *IEEE Commun. Surv. Tut.*, vol. 26, no. 4, pp. 2213–2257, Fourthquarter 2024.
- [10] M. Cui and L. Dai, "Channel estimation for extremely large-scale MIMO: Far-field or near-field?" *IEEE Trans. Commun.*, vol. 70, no. 4, pp. 2663–2677, Apr. 2022.
- [11] D. Gürgünoğlu *et al.*, "Performance analysis of a 2D-MUSIC algorithm for parametric near-field channel estimation," *IEEE Wireless Commun. Lett.*, Mar. 2025, Early Access.